J Appl Electrochem (2011) 41:1183–1190
DOI 10.1007/s10800-011-0343-7

ORIGINAL PAPER

Acceleration of the redox kinetics of VO^{2+}/VO_2^+ and V^{3+}/V^{2+} couples on carbon paper

Xiong Wei Wu · Tomoo Yamamura · Suguru Ohta · Qi Xiu Zhang · Fu Cong Lv · Can Ming Liu · Kenji Shirasaki · Isamu Satoh · Tatsuo Shikama · Dan Lu · Su Qin Liu

Received: 26 April 2011 / Accepted: 30 July 2011 / Published online: 6 September 2011

Abstract The redox kinetics of VO^{2+}/VO_2^+ and V^{3+}/V^{2+} couples on a carbon paper (CP, HCP030 N, Shanghai Hesen, Ltd., China) electrode were investigated in terms of their standard rate constant (k_0) and reaction mechanism. The values determined for k_0 for $VO^{2+} \rightarrow VO_2^+$ and $V^{3+} \rightarrow V^{2+}$ using the CP electrode are 1.0×10^{-3} and 1.1×10^{-3} cm s^{-1}, respectively. The value of k_0 increases by one or two order(s) of magnitude compared with values obtained using electrodes composed of pyrolytic graphite and glassy carbon. The acceleration of the redox kinetics of vanadium ions is a result of the large surface area of the CP electrode. An inner-sphere mechanism for the reaction on the surface of the electrode is proposed. The kinetic features of vanadium redox reactions on the CP electrode reveal that CP is suitable for use as the electrodes in vanadium redox-flow batteries.

Keywords Carbon paper · Vanadium redox reaction · Standard rate constants · Oxygen content · Vanadium redox-flow battery

X. W. Wu (✉) · F. C. Lv · D. Lu · S. Q. Liu
School of Chemistry and Chemical Engineering, Central South University, Changsha 410083, China
e-mail: wxwcsu@yahoo.cn

T. Yamamura · S. Ohta · K. Shirasaki · I. Satoh · T. Shikama
Institute for Materials Research, Tohoku University, Sendai, Miyagi 980-8577, Japan

Q. X. Zhang
School of Metallurgical Science and Engineering, Central South University, Changsha 410083, China

C. M. Liu
Hunan Agricultural University, Changsha 410128, China

1 Introduction

The vanadium redox-flow battery (VRB) proposed by Skyllas-Kazacos and coworkers [1, 2] has unique advantages such as low cost, long cycle life, deep-discharge capacitance and large-scale applicability in addition to a high energy efficiency of 82.3% with voltage efficiency of 85.1% [3]. This technology has attracted great interest [4–8] and several VRB systems for practical application have been demonstrated. A VRB system with 4 MW/6 MWh has been installed at a wind power station in Tomamae, Hokkaido, Japan. The energy efficiency of VRBs is significantly influenced by the kinetic properties of the electrodes because the battery uses solution-based active materials. Shiokawa et al. have shown that the energy efficiency of charge–discharge cycles of VRB systems is dependent on the standard rate constant k_0 for the redox reactions [9, 10]. The energy efficiency decreases rapidly from 99 to 60% when k_0 is reduced from $\sim 10^{-1}$ to $\sim 10^{-4}$ cm $s^{-}1$ at a current density of 80 mA cm^{-2}. The redox kinetics of the VO^{2+}/VO_2^+ and V^{3+}/V^{2+} couples were first determined by Sum and Skyllas-Kazacos on glassy carbon (GC) to be $k_0 = 7.5 \times 10^{-4}$ and 1.7×10^{-5} cm s^{-1}, respectively [1, 2]. These k_0 values indicate that both the VO^{2+}/VO_2^+ and V^{3+}/V^{2+} couples are irreversible on GC. In addition, Yamamura and coworkers determined k_0 for the VO^{2+}/VO_2^+ and V^{3+}/V^{2+} couples on plastic-formed carbon (PFC) and pyrolytic graphite (PG), and found that k_0 improved for both couples on these electrodes but still exhibited irreversible behavior [11].

Graphite fiber felt has been used on both the positive and negative sides of VRBs [12]. The basic unit of graphite fiber is a layered carbon network composed of hexagonal rings; the function of graphite fiber is thus similar to PG. Sun and Skyllas-Kazacos found that graphite materials

modified by thermal or acid treatment showed improved properties [12–14], which was attributed to an increase in the amount of oxygen atoms on the graphite surface. This finding indicates that oxygen atoms are involved in the reactions of the electrodes.

Recently, carbon paper (CP) has been widely used as an electrode in fuel cells [15–18], lithium ion batteries [19], and super capacitors [20]. The characteristics of CP, such as its high porosity (greater than 70%), low density (0.5 g cm^{-3}), thinness (0.3 mm) and small electrical resistance (0.005 Ω cm) [15, 18], make it a promising electrode material for VRBs. Using CP as an electrode material, Liu and coworkers constructed a VRB system that achieved high current efficiency (95%) and voltage efficiency (82%) at a current density of 20 mA cm^{-2} [21]. A study on the reaction kinetics of the Fe^{2+}/Fe^{3+} redox couple [22] revealed that electron transfer is the rate-determining step. However, the standard rate constants of the VO^{2+}/VO_2^{+} and V^{3+}/V^{2+} couples on CP have not been determined to date. Furthermore, it is worthwhile to compare the values of k_0 on CP with those obtained using other carbon electrodes.

In comparison with the polymer electrolyte fuel cell (PEFC) application, there are different several considerations of electrode materials for flow battery application; (i) high electrochemical activity, (ii) high gas evolution overpotential, (iii) high surface area, and (iv) low flow resistance. In the VRB application, the concentration of vanadium ions may be two or three order magnitude lower than H_2 or O_2 activity in PEFC. Also, liquid viscosity is significantly higher than gas viscosity. Thus thin electrode, of which the thickness is typically less than 0.3 mm for PEFC, may not be suitable for flow battery application due to high flow resistance. Carbon paper is stiffer than felt, which may result in high electrical contact resistance for the same assembly condition. The stiffness and the hydrophobicity are designed for the application. In this paper, we present the fundamental kinetic study on the CP material for the VRB application, which can be compared with VSSB (Vanadium Solid-Salt Battery) proposed by us [23]. In the VSSB application, the vanadium solid salt was included and the concentration of the vanadium is up to 15 times of the VRB. Therefore, this kind of the fundamental kinetic study is useful for the VRB and also for the VSSB.

Because it is a promising electrode material, CP was used to study the electrochemistry of vanadium couples for potential use as an electrode in a VRB. The kinetics of the VO^{2+}/VO_2^{+} and V^{3+}/V^{2+} couples were investigated on a CP electrode. The obtained standard rate constants were compared with those determined on other carbon-based electrodes and the electrode reaction mechanism was discussed.

2 Experimental

2.1 Materials

Chemicals such as $VOSO_4 \cdot nH_2O$ and sulfuric acid were purchased from Wako Pure Chemical Industries, Ltd., Osaka, Japan. Solutions of vanadium in sulfuric acid were prepared by a method described previously [11]. Electrochemical reduction of V^{4+} to V^{3+} was performed under a constant voltage using a galvanostat (HA-501, Hokuto Denko Co., Tokyo, Japan). The hydration number n of $VOSO_4 \cdot nH_2O$ was determined to be $n = 3.75$ using an ICP-AES spectrophotometer (ICPS-7500, Shimadzu Corp., Kyoto, Japan).

CP (Product code HCP030 N) was purchased from Shanghai Hesen, Ltd., Shanghai, China. The specific surface area of CP was determined by Brunauer–Emmet–Teller (BET) adsorption measurements obtained using a FlowSorb III 2305 surface area analyzer (Shimadzu Corp., Kyoto, Japan). BET values were also measured for CPs (Product codes TGP-H-060 and TGP-H-120) purchased from Toray Industries Inc., Tokyo, Japan.

2.2 Measurements

Cyclic voltammetry was conducted using an electrochemical analyzer (HZ-3000, Hokuto Denko Co., Tokyo, Japan) with a reference electrode (Ag/AgCl), and counter electrode (10 × 10 mm platinum plate). 1ϕ GC and 3ϕ c plane of pyrolystic graphite (c-PG) electrodes were purchased from BAS Inc., Tokyo, Japan. The electrodes were activated by polishing their surfaces with α-alumina (0.05 μm), and then rinsing with distilled water in an ultrasonic cleaner for 5 min. The CP electrode was prepared by punching out a piece of CP with a thickness of 280 μm into a 3ϕ disc. The disc was attached on the top of a 10ϕ rod that brass alloy rod did wrap by a PEEK resin, poly(ether ether ketone), using an adhesive (Ag paste). The prepared CP electrode was dried under vacuum for 3 h. The carbon surface was activated by cycling between −0.2 and 1.2 V versus Ag/AgCl for 30 min.

We checked the electrode by cyclic voltammograms of $Fe(CN)_6^{3-}/Fe(CN)_6^{4-}$ with an electrolyte of 2.0 mol dm^{-3} Na_2SO_4 (Fig. 1). It is known that the half-wave potential of this couple is susceptible to be influenced by electrode materials and electrolytes. The determined $E_{1/2}$ values of ~0.24 V vs. Ag/Ag^+ on CP, c-PG and GC electrodes agree very well with the reported value of the standard potential (0.26 V vs. Ag/Ag^+) for $Fe(CN)_6^{3-}/Fe(CN)_6^{4-}$ couple in 0.5 mol dm^{-3} Na_2SO_4 [24].

The surfaces of the CP, c-PG and GC samples were observed using a scanning electron microscope (SEM, JSM-6390A, JEOL, Tokyo, Japan) equipped with an

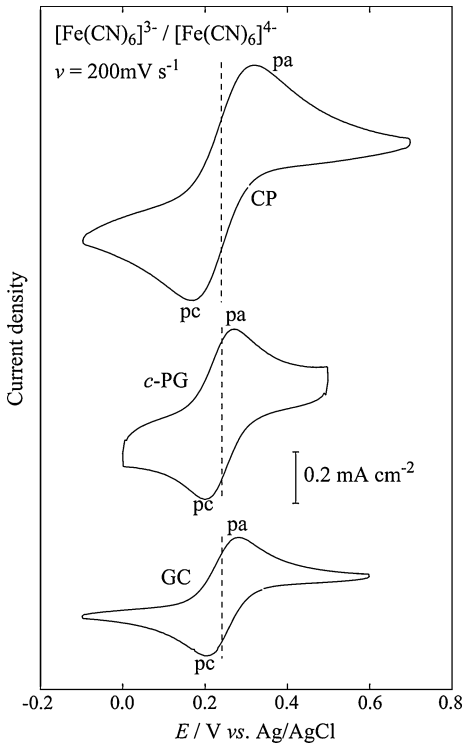

Fig. 1 Cyclic voltammograms of aqueous solution of 1.0×10^{-3} mol dm^{-3} $Fe(CN)_6^{3-}/Fe(CN)_6^{4-}$ with an electrolyte of 2.0 mol dm^{-3} Na_2SO_4 on CP, *c*-PG and GC electrode at scan rate of 200 mV s^{-1}. Voltammograms at fifth scan is shown. *Vertical dashed lines* indicate the value of $E_{1/2}$. Current density is evaluated based on geometric area of electrode surface

energy-dispersive X-ray (EDX) analyzer. Prior to SEM observation, the electrodes containing rods made of PEEK were cut to restrict the height of the rods to less than 5 mm.

3 Results and discussion

3.1 Morphology of CP

An SEM micrograph of the surface of HCP030 N is shown in Fig. 2. The surface is composed of overlapping needle-shaped carbon fibers over a base of multiple layers by binder. Such a surface structure has a large effective surface area. The specific surface area obtained by the BET method is the surface area measured by the adsorption of gasses. The surface area by the BET is considered to be related to the effective area evaluated by the surface electrochemical reaction of vanadium ions. Compared with the CPs from Toray (TGP-H-060) [22], the HCP030 N sample has fewer fibers. However, this does not mean that the HCP030 N has a lower specific surface area than the CP from Toray (TGP-H-060). The specific surface area measured for HCP030 N is 10.9 m^2 g^{-1}, which is consistent with the reported value [25], compared with 5.5 and

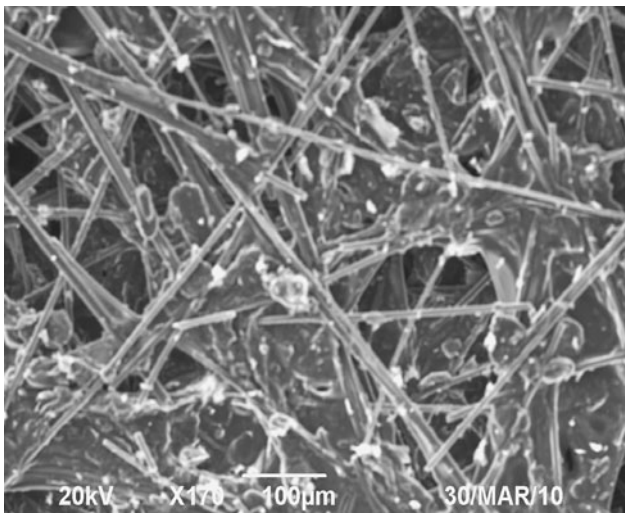

Fig. 2 SEM image of CP (HCP030 N) at a magnification of ×170

5.8 m^2 g^{-1} for TGP-H-060 and TGP-H-120, respectively. Based on the average weight of 3ϕ CP (1.171 ± 0.128 mg) used in this study, the specific surface area of the electrode is 1.28×10^2 cm^2. The ratio of the specific surface area to the geometric area is 1.80×10^5.

3.2 Redox kinetics of V^{3+}/V^{2+} on CP

Typical cyclic voltammograms for the redox reaction of the V^{3+}/V^{2+} couple in an electrolyte of 1.0 mol dm^{-3} H_2SO_4 using HCP030 N, *c*-PG and GC electrodes at a scan rate of 200 mV s^{-1} are shown in Fig. 3. The large peak separations using the *c*-PG (875 mV) and GC (1027 mV) electrodes are characteristic of irreversible (IR) behavior according to previous studies [1, 11, 26]. In contrast, the cyclic voltammogram obtained on the HCP030 N electrode exhibits the characteristic features of quasi-reversible (QR) behavior: small peak separation (288 mV) and a large peak current that is 2.4 and 20.9 times larger than those on the *c*-PG and GC electrodes, respectively. The half-wave potential for the V^{3+}/V^{2+} couple on the CP electrode ($E_{1/2} = -0.498$ V vs. Ag/AgCl) agrees well with the standard potential of −0.454 V versus Ag/AgCl [27] and also with the values obtained using *c*-PG (−0.475 V) and GC (−0.469 V) electrodes (Table 1).

When the scan rate is increased from 10 to 200 mV s^{-1} (Fig. 4), the peak separation ΔE_p on the HCP030 N electrode increases from 61 to 288 mV, and the V^{3+}/V^{2+} redox couple still exhibits QR behavior. The diffusion constant D of V^{3+} determined on the HCP030 N electrode (1.41×10^{-5} cm^2 s^{-1}) from the relationship shown in Fig. 5a is very large compared with that on the *c*-PG electrode ($D = 4.93 \times 10^{-6}$ cm^2 s^{-1}) and values reported for *c*-PG (4.0×10^{-6} cm^2 s^{-1} [11]), GC (1.41×10^{-6} cm^2 s^{-1} [1] and 5.2×10^{-6} cm^2 s^{-1} [26]), and PFC (2.4×10^{-6} cm^2 s^{-1}

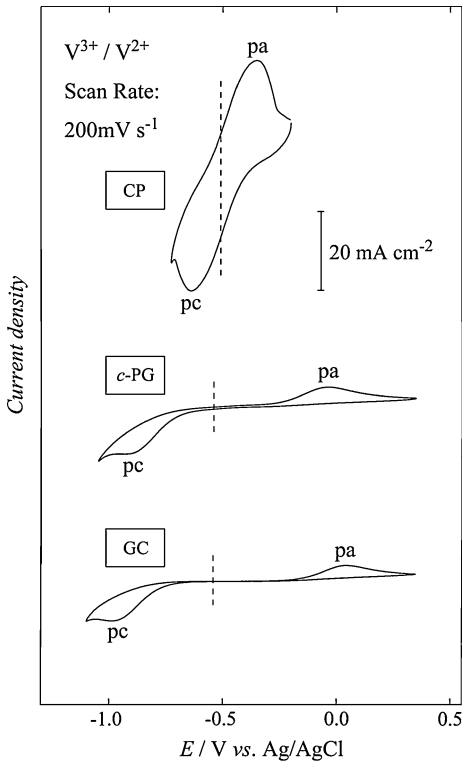

Fig. 3 Cyclic voltammograms obtained in an aqueous solution containing 5.0×10^{-2} mol dm^{-3} V^{3+} in an electrolyte of 1.0 mol dm^{-3} H_2SO_4 using CP, *c*-PG and GC electrodes at a scan rate of 200 mV s^{-1}. Voltammograms shown are of the fifth scan. *Vertical dashed lines* indicate $E_{1/2}$. The current density was evaluated based on the geometric area of each electrode surface

[11]). As discussed above, the effective surface area (A in Eq. 1), is underestimated if it is assumed to be the geometrical area of the HCP030 N electrode. If $D = 4.0 \times 10^{-6}$ cm^2 s^{-1} [11], where we used this value because of almost the middle among the values appeared in the literatures, is used as a standard value for V^{3+} ions, the effective value calculated for is $A = 0.133$ cm^2, which is about 20 times larger than the actual geometric area (0.07 cm^2). Using $D = 4.0 \times 10^{-6}$ cm^2 s^{-1}, a value of $k_0 = 1.07 \times 10^{-3}$ cm^2 s^{-1} was obtained from Fig. 6a using the Nicholson function Ψ [27]. The obtained k_0 value on CP is larger than the k_0 values obtained on *c*-PG, GC, and PFC.

Because ΔE_p (0.288 V at 200 mV s^{-1}) is on the borderline between QR and IR behavior, both D and k_0 were determined based on an IR system in addition to the above-mentioned treatment based on a QR system. For an IR system, i.e., for reactions with $\Delta E_p > 250$ mV, D and k_0 are given by

$$I_p = 2.99 \times 10^5 \cdot AC_0(\alpha D v)^{\frac{1}{2}} \quad (1)$$

$$\ln I_p = \ln(0.227 \cdot FAC_0 k_0) - \frac{\alpha n}{RT}\left(E_p - E^{0'}\right) \quad (2)$$

where α is the transfer coefficient, E_p is the cathodic or anodic peak potential, and $E^{0'}$ is the standard potential. A similar calculation using $D(V^{3+}) = 4.0 \times 10^{-6}$ cm^2 s^{-1} [11] gives $k_0 = 1.13 \times 10^{-3}$, which closely agrees with the value obtained for QR treatment. This finding supports the conclusion that the system lies on the borderline between QR and IR behavior. The values determined for D and k_0 for the CP, *c*-PG and GC electrodes are summarized in Table 1, along with literature values. Considering the Nernst relation, the Relationship between k_0 and exchange current density i_0 was described following equation [see ref. 25].

$$i_0 = Fk_0 C_O^{*(1-\alpha)} C_R^{*\alpha} \quad (3)$$

where C_O^* is bulk concentration of oxidative species, C_R^* is bulk concentration of reductive species. For the particular case where $C_O^* = C_R^* = C$ ($\alpha = 0.5$; in reversible system)

$$i_0 = Fk_0 C \quad (4)$$

The results show that the electrode kinetics of the V^{3+}/V^{2+} couple on the HCP030 N electrode are accelerated by one or two order(s) of magnitude compared with on GC, *c*-PG and other electrodes.

3.3 Redox kinetics of VO^{2+}/VO_2^+ on CP

Typical cyclic voltammograms for the VO^{2+}/VO_2^+ couple in an electrolyte of 1.0 mol dm^{-3} H_2SO_4 obtained using HCP030 N, *c*-PG and GC electrodes at a scan rate of 200 mV s^{-1} are shown in Fig. 7. The peak separation for the redox reaction using the HCP030 N electrode (227 mV), which is notably smaller than those observed using *c*-PG (945 mV) and GC (1450 mV) electrodes at 200 mV s^{-1}, shows the QR nature of the VO^{2+}/VO_2^+ couple on the HCP030 N electrode. From the variation of the peak current density (I_p) at various scan rates (Fig. 8), a linear correlation versus $v^{1/2}$ (Fig. 5b) gave a value of D of 1.79×10^{-7} cm^2 s^{-1}, which is just 25% of those obtained on *c*-PG ($D = 6.30 \times 10^{-6}$ cm^2 s^{-1}), GC ($D = 6.81 \times 10^{-6}$ cm^2 s^{-1}) and other electrodes (Table 2). The underestimation of surface area was corrected to give $A = 0.019$ cm^2 for QR and 0.028 cm^2 for IR behavior by adopting $D = 2.4 \times 10^{-6}$ cm^2 s^{-1} for VO^{2+} [11]. A plot of Ψ versus $v^{-1/2}$ for the CP electrode (Fig. 6b) gives k_0 values of 8.79×10^{-4} (QR) and 1.04×10^{-3} (IR), which are 6–10 times larger than those obtained using other electrodes (Table 2). The results show that the standard rate constant on the CP electrode is increased by one order of magnitude for the VO^{2+}/VO_2^+ couple compared with GC and *c*-PG electrodes. As a result of this acceleration, the value of k_0 for VO^{2+}/VO_2^+ on the HCP030 N electrode is similar to that observed for the V^{3+}/V^{2+} couple.

Table 1 Electrochemical properties (half-wave potential $E_{1/2}$, difference ΔE_p, reversibility CR, standard rate constant k_0 and diffusion constant D) of the $V^{3+} \rightarrow V^{2+}$ reaction on various electrodes

Electrode	Size of electrode (ϕ)	[V] (mol dm^{-3})	$E_{1/2}$[d]/V vs. Ag/AgCl	ΔE_p[d]/V	CR	D (cm^2 s^{-1})	k_0 (cm s^{-1})	Ref.
CP	3	0.05[a]	−0.495	0.288	IR[g]	4.0×10^{-6}[h]	1.13×10^{-3}[h]	This work
						(3.35×10^{-5})[i]	(3.28×10^{-3})[i]	
					QR[g]	4.0×10^{-6}[h]	1.07×10^{-3}[h]	
						(1.41×10^{-5})[i]	(2.01×10^{-3})[i]	
c-PG	3	0.05[a]	−0.507	0.618	IR	4.0×10^{-6}	5.5×10^{-4}	[11]
		0.05[a]	−0.475	0.875	IR	4.93×10^{-6}	3.50×10^{-5}	This work
GC	3	0.12[a]	−0.55[e]	0.44[e]	IR	1.41×10^{-6}	1.7×10^{-5}	[1]
		0.005[b]		0.304		5.2×10^{-6}	$(8.7 \pm 0.3) \times 10^{-4}$	[24]
	1	0.05[a]	−0.469	1.03	IR	8.45×10^{-6}	5.40×10^{-5}	This work
GRC	0.5	0.05[c]	−0.58[f]	0.09[f]	QR	NS[k]	9.7×10^{-3}	[31]
					IR	5.0×10^{-6}[g]	5.2×10^{-4}[j]	[11]
PFC	1	0.05	−0.51[f]	0.64[f]	IR	2.4×10^{-6}	5.3×10^{-4}	[11]

GRC graphite-reinforced carbon, *CR* classification of reversibility, *QR* quasi-reversible, *IR* irreversible

[a] $[H_2SO_4] = 1$ mol dm^{-3}

[b] $[HClO_4] = 0.3$ mol dm^{-3}

[c] $[H_2SO_4] = 3$ mol dm^{-3}

[d] Scan rate of 200 mV s^{-1}

[e] Scan rate of 10 V min^{-1}

[f] Value read from Fig. 2 in ref. [31]

[g] Because ΔEp (0.288 V) is on the borderline between QR and IR behavior, analyses based on both QR and IR were applied

[h] $D = 4.0 \times 10^{-6}$ cm^2 s^{-1} from ref. [11] was used (see text)

[i] The surface area is the geometrical area (3ϕ)

[j] Reanalyzed data in ref. [31] using values in ref. [11]

[k] Not shown

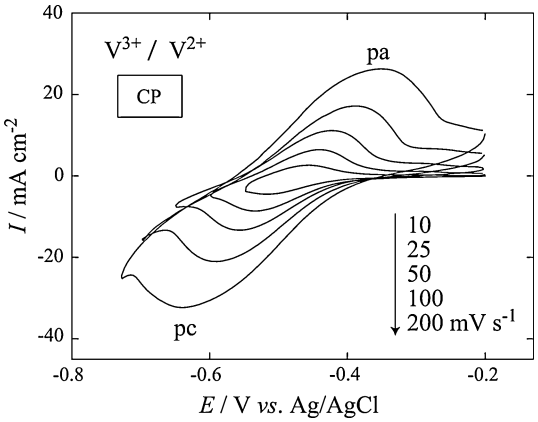

Fig. 4 Cyclic voltammograms obtained in an aqueous solution containing 5.0×10^{-2} mol dm^{-3} $V3^+$ in an electrolyte of 1.0 mol dm^{-3} H_2SO_4 using a CP electrode at various scan rates of 10, 25, 50, 100 and 200 mV s^{-1}. Voltammograms shown are of the fifth scan. The current density was evaluated based on the geometric area of the electrode surface

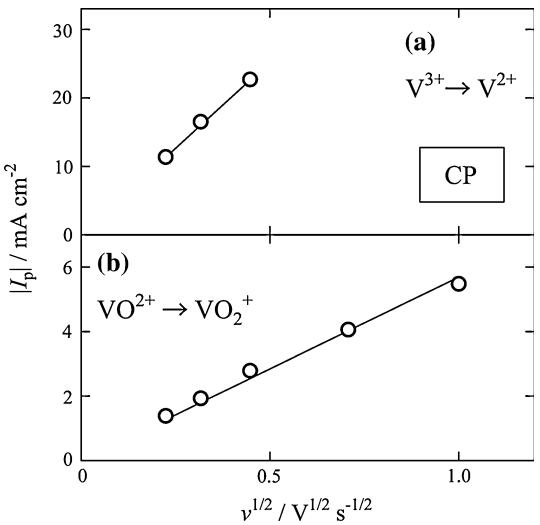

Fig. 5 Peak current density (I_p) versus $v^{1/2}$ obtained using a CP electrode for the redox couples **a** $V^{3+} \rightarrow V^{2+}$, and **b** $VO^{2+} \rightarrow VO_2^+$ in electrolytes of 1.0 mol dm^{-3} H_2SO_4. The current density was evaluated based on the geometric area of the electrode surface

3.4 Reaction mechanism of VO^{2+}/VO_2^+ on CP

As shown in Fig. 7, a cyclic voltammogram of the VO^{2+}/VO_2^+ couple using the *c*-PG electrode shows two redox waves ($E_{pa} = 1.233$ V and $E_{pc} = 0.288$ V vs. Ag/AgCl) with a half-wave potential $E_{1/2}$ of 0.760 V versus Ag/AgCl. The value of $E_{1/2}$ is close to the standard electrode potential

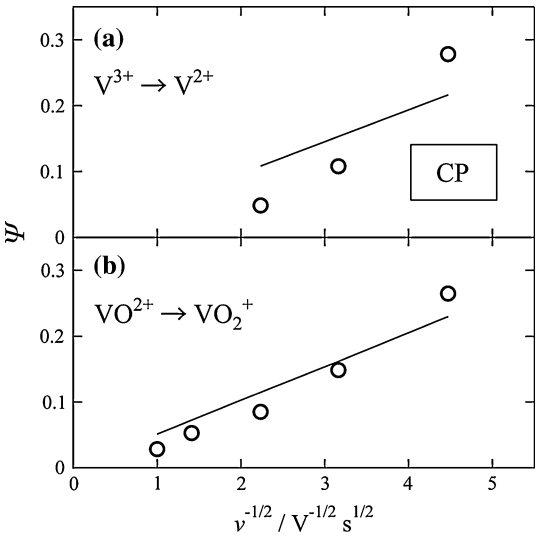

Fig. 6 Ψ versus $v^{-1/2}$ obtained using a CP electrode for the redox couples: **a** $V^{3+} \rightarrow V^{2+}$, and **b** $VO^{2+} \rightarrow VO_2^{+}$, in an electrolyte of 1.0 mol dm^{-3} H_2SO_4

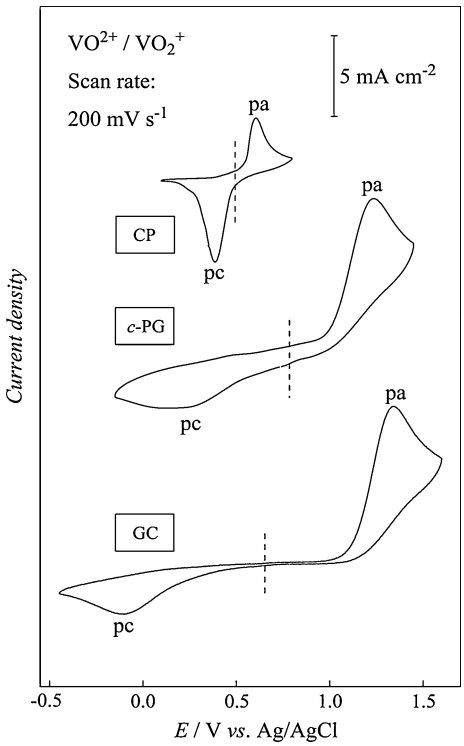

Fig. 7 Cyclic voltammograms obtained for an aqueous solution containing 5.0×10^{-2} mol dm^{-3} V^{4+} in an electrolyte of 1.0 mol dm^{-3} H_2SO_4 using CP, *c*-PG and GC electrodes at a scan rate of 200 mV s^{-1}. Voltammograms shown are of the fifth scan. *Vertical dashed lines* indicate $E_{1/2}$. The current density was evaluated based on the geometric area of each electrode surface

of VO^{2+}/VO_2^{+} of 0.8 V versus Ag/AgCl [27] derived from the Gibbs free energy of the VO^{2+}/VO_2^{+} reaction in acidic solution:

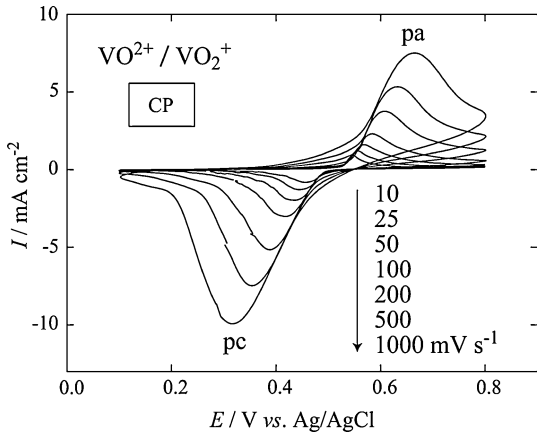

Fig. 8 Cyclic voltammograms obtained for an aqueous solution containing 5.0×10^{-2} mol dm^{-3} V^{4+} in an electrolyte of 1.0 mol dm^{-3} H_2SO_4 on a CP electrode at various scan rates of 10, 25, 50, 100 and 200 mV s^{-1}. Voltammograms shown are of the fifth scan. The current density was evaluated based on the geometric area of the electrode surface

$$VO^{2+} + H_2O \rightarrow VO_2^{+} + 2H^{+} + e^{-} \quad (5)$$

This *standard* reaction exhibits a slow outer-sphere mechanism and proceeds via (i) release of an electron by $[V{=}O]^{2+}$ and (ii) formation of a monovalent cation $[O{=}V{=}O]^{+}$ by release of two protons [28, 29] (Mechanism A, Fig. 9). The corresponding redox reaction, i.e., electron exchange in solution, has been studied by ^{17}O NMR spectroscopy and was attributed to inner-sphere processes including a very rapid pre-equilibrium between VO^{2+} and VO_2^{+} to form a mixed-valence $V_2O_3^{3+}$ species that undergoes rapid electron exchange with VO^{2+} (Mechanism B, Fig. 9) [30–32]. Yamamura also classified the electrode reaction as a slow outer-sphere mechanism [11].

On the other hand, the $E_{1/2}$ values of the VO^{2+}/VO_2^{+} couple obtained using GC and CP electrodes are remarkably shifted from the standard potential of 0.8 V at 0.621 and 0.499 V versus Ag/AgCl, respectively (Fig. 7). If the $E_{1/2}$ value obtained using the *c*-PG electrode is assumed to be the reference, the shift for the GC electrode is 141 mV and that for the CP electrode is 261 mV. These large shifts can be attributed to the different inner-sphere species involved in the reactions at the electrode surface.

That the reaction mechanism occurs via an inner-sphere species, as illustrated in Fig. 9 (Mechanism C or D), is also supported by our previous study. The infrared absorption attributed to carbonyl (–C=O) and hydroxyl (–OH) groups increased after acid treatment. The previous result suggests that oxygen may be involved in the electrode reaction [21]. These findings are similar to the results reported by Sun and Skyllas-Kazacos [13, 14].

Table 2 Electrochemical properties (half-wave potential $E_{1/2}$, difference ΔE_p, reversibility CR, standard rate constant k_0 and diffusion constant D) of the $VO^{2+} \rightarrow VO_2^+$ reaction on various electrodes

Electrode	Size of electrode (ϕ)	[V] (mol dm^{-3})	$E_{1/2}^c$/V vs. Ag/AgCl	E_{pa}^c/V vs. Ag/AgCl	E_{pc}^c/V vs. Ag/AgCl	ΔE_p^c/V	CR	D (cm^2 s^{-1})	k_0 (cm s^{-1})	Ref.
CP	3	0.05[a]	0.498	0.611	0.384	0.227	IR[f]	2.4×10^{-6}[g] (3.75×10^{7})[h]	1.04×10^{-3}[g] (4.10×10^{4})[h]	This work
							QR[f]	2.4×10^{-6}[g] (1.79×10^{-7})[h]	8.79×10^{4}[g] (2.40×10^{4})[h]	
	0.739 cm^2	0.2[b]	0.91				IR	7.75×10^{-5}	2.52×10^{-4}	[32]
c-PG	3	0.05[a]	0.77[d]	1.13	0.41	0.72[d]	IR	2.4×10^{-6}	1.3×10^{-4}	[11]
		0.05[a]	0.76	1.233	0.287	0.945	IR	6.30×10^{-6}	5.17×10^{-5}	This work
GC	3	0.055 (pH 4 to −0.5)	0.81[e]	1.51	0.11	1.4[e]	IR	1.4×10^{-6}	7.5×10^{-4}	[2]
	1	0.05[a]	NS[j]			NS[j]		2.8×10^{-6}	6.8×10^{-5}	[11]
		0.05[a]	0.621	1.346	−0.104	1.45	IR	6.81×10^{-6}	1.30×10^{-5}	This work
Pt		0.01[a]						Not determined	1.4×10^{-5}	[33]
GRC	0.5	0.05[b]	0.81[d]	0.97	0.65	0.32[d]	IR	4.1×10^{-6}[i]	5.2×10^{-4}[i]	[31]
PFC	1	0.05[a]	DD[k]			DD[k]	IR	3.9×10^{-6}	8.5×10^{-4}	[11]

GRC graphite-reinforced carbon, *CR* classification of reversibility, *QR* quasi-reversible, *IR* irreversible

[a] $[H_2SO_4] = 1$ mol dm^{-3}

[b] $[HClO_4] = 0.3$ mol dm^{-3}

[c] Scan rate of 200 mV s^{-1}

[d] Value read from Fig. 2 in ref. [31]

[e] Scan rate of 10 V min^{-1}

[f] Because ΔEp (0.227 V) is on the borderline between QR and IR behavior, analyses based on both QR and IR were applied

[g] $D = 2.4 \times 10^{-6}$ cm^2 s^{-1} from ref. [11] was used (see text)

[h] The surface area is the geometrical area (3ϕ)

[i] Reanalyzed data from ref. [31] using values in ref. [11]

[j] Not shown

[k] Difficult to determine

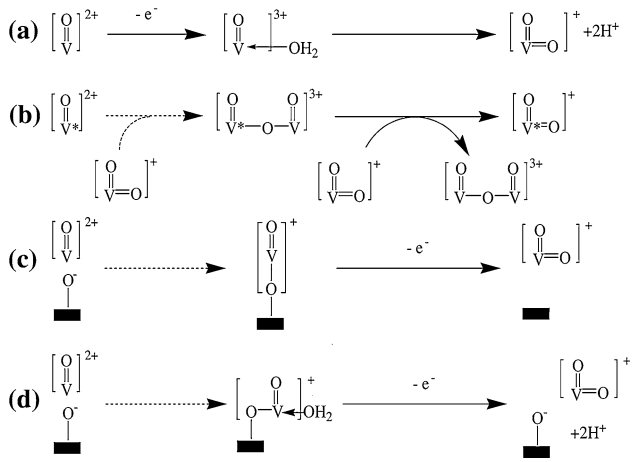

Fig. 9 Proposed mechanisms for the reaction of the VO^{2+}/VO_2^+ redox couple on the surface of a CP electrode as well as a rapid electron exchange mechanism [31, 32]. *Black rectangles* correspond to a layered carbon network of CP. *Asterisks* indicate identical atoms indistinguishable by NMR spectroscopy [32]

4 Conclusions

The standard rate constants of the VO^{2+}/VO_2^+ and V^{3+}/V^{2+} redox couples on a CP (HCP030 N) electrode were measured to assess CP as a new electrode material in VRBs. On the CP electrode, the electrode kinetics of the V^{3+}/V^{2+} and VO^{2+}/VO_2^+ couples were accelerated by two and one order(s) of magnitude, respectively, compared with those obtained on other electrodes (*c*-PG and GC). As a result of this acceleration, k_0 is 1×10^{-3} cm s^{-1} for both the V^{3+}/V^{2+} and VO^{2+}/VO_2^+ couples. The acceleration of the redox kinetics of vanadium ions was attributed to (i) the large surface area of HCP030 N, and (ii) an inner-sphere mechanism for the reaction on the surface of the CP electrode.

Acknowledgments We thank Mr. M. Takahashi from the Institute for Materials Research (IMR), Tohoku University, for his kind assistance. All experiments were performed at the Experimental

Facility for Alpha-Emitters of IMR, Tohoku University. We also thank Prof. Y. P. Wu from Fudan University, Shanghai, China. This work was partly supported by the Ministry of Education, Science, Sports and Culture, Grant-in-Aid for Scientific Research (B) 22360408 from Japan Society for the Promotion of Science (JSPS). The research was partly supported by the National Basic Research Program of China (973 Program No: 2010CB227201) and National Science Foundation Committee of China (50972165).

References

1. Sum E, Skyllas-Kazacos M (1985) J Power Sources 15:179
2. Sum E, Rychcik M, Skyllas-Kazacos M (1985) J Power Sources 16:85
3. Tokuda N, Kanno T, Hara T et al (2000) SEI Technical Review 50:88
4. Hagg CM, Skyllas-Kazacos M (2002) J Appl Electrochem 32:1063
5. Kausar N, Howe R, Skyllas-Kazacos M (2001) J Appl Electrochem 31:1327
6. Sukkap T, Skyllas-Kazacos M (2004) J Appl Electrochem 34:137
7. Fang B, Wei Y, Kumagai Y (2003) J Appl Electrochem 33:197
8. Haddadi-asl V, Kazacos M, Skyllas-Kazacos M (1995) J Appl Electrochem 25:29
9. Hasegawa K, Yamamura T, Shiokawa Y et al (2005) J Phys Chem Solids 66:593
10. Yamamura T, Watanabe N, Shiokawa Y (2006) J Alloys Compd 408–412:1260
11. Yamamura T, Watanabe N, Shiokawa Y et al (2005) J Electrochem Soc 152:A830
12. Zhong S, Kazacos M, Skyllas-Kazacos M (1993) J Power Sources 45:29
13. Sun B, Skyllas-Kazacos M (1992) Electrochim Acta 37:1253
14. Sun B, Skyllas-Kazacos M (1992) Electrochim Acta 37:2459
15. Saha MS, Li R, Sun X et al (2009) Electrochem Commun 11:438
16. Liu CH, Ko TH, Liao YK (2008) J Power Sources 178:80
17. Maheshwari PH, Mathur RB, Dhami TL et al (2008) Electrochim Acta 54:655
18. Mathur RB, Maheshwari PH, Dhami TL et al (2006) J Power Sources 161:790
19. Arbizzani C, Beninati S, Lazzari M et al (2005) J Power Sources 141:149
20. Chou SL, Wang JZ, Chew SY et al (2008) Electrochem Commun 10:1724
21. Liu SQ, Shi XH, Wu XW et al (2008) Chinese J Inorg Chem 24:1079
22. Khosravi M, Amini MK (2010) Carbon 48:3131
23. Yamamura T, Wu X, Ohta S, Shirasaki K, Sakuraba H, Satoh I, Shikama T, Power J (2011) Sources 196:4003–4011
24. Kulesza P, Jedral T, Galus Z (1980) J Electroanal Chem 109:141–149
25. Li JX, Steigerwalt ES, Sambandam S et al (2007) Chem Mater 19:6001
26. McDermott CA, Kneten KR, McCreery RL (1993) J Electrochem Soc 140:2593
27. Bard AJ, Faulkner LR (2000) Electrochemical methods: fundamentals and applications. Wiley, New York
28. Macartney DH (1986) Inorg Chem 25:2222
29. Gattrell M, Park J, MacDougall B et al (2004) J Electrochem Soc 151:A123
30. Giuliano CR, McConnell HM (1959) J Inorg Nucl Chem 9:171
31. Blanc P, Madic C, Launay JP (1982) Inorg Chem 21:2923
32. Okamoto K, Tomiyasu H, Fukutomi H et al (1988) Inorg Chim Acta 143:217
33. Kaneko H, Nozaki K, Wada Y et al (1991) Electrochim Acta 36:1191